*Supplementary information for*

# Rational Design of Halo-imidazolium-based Ionic Liquids: Tailoring the Charge Distribution to Mimic the Structure of Real Charge Inverted Analogues

*Lois Morandeira,*[a,b] Tiago F. C. Cruz,[a] Pedro T. Gomes,[a] José N. Canongia Lopes[a] and Karina Shimizu*[,*]*

[a] Centro de Química Estrutural, Departamento de Engenharia Química, Instituto Superior Técnico, Universidade de Lisboa, 1049-001, Lisboa (Portugal)

[b] CINTECX, Department of Chemical Engineering, University of Vigo, 36310, Vigo (Spain)

AUTHOR INFORMATION

**Corresponding Author**

[*] Lois Morandeira – ORCID: 0000-0002-3646-0899 // email: lmorandeira@uvigo.gal

[*] Karina Shimizu – ORCID: 0000-0003-2454-1795 // email: karina.shimizu@tecnico.ulisboa.pt

# Table of Contents

## 1. Background for the modification of imidazolium- and cyclopentadienyl-like structures

Before tackling the study of one of the pairs arising from the fluorination of both the cyclopentadienyl (Cp) and imidazolium (Im) cores ($[C_4C_1F_3Im]^+$ with $[C_4C_1Cp]^-$ (Figures S2A and S2D) and $[C_4C_1F_3Cp]^-$ with $[C_4C_1Im]^+$ (Figures S2B and S2C)), we reviewed the existing literature on the synthesis of 1,3-dialkyl-2,4,5-trifluoro-Im or Cp.

On one hand, there are numerous examples in the literature where the Cp moiety has been modified with a variety of organic substituents.[1–6] Unfortunately, those addressing the halogenation of the Cp core are scarce[7,8] and, to the best of our knowledge, there have been no reports on the halogenation of 1,3-dialkyl-Cp anions. In this sense, it is worth noting that, despite the structure and chemistry of common (hydrogenated) Cp anions has been widely studied,[9] the dialkyl versions were firstly presented a couple of years ago.[10,11]

On the other hand, the modification of the imidazolium (Im) core is a well-explored topic, with a wide range of structures already reported in the literature. For example, the modification of imidazoles/imidazoliums with organic and inorganic substituents has been extensively studied, due to their significant applications in biology, catalysis[12–14] and as precursors to the ubiquitous *N*-heterocyclic carbene ligands.[15–17] In the context of Im-based compounds structurally related to ionic liquids (ILs), the interest in modifying the heterocyclic core, both the modification *per se* and its usability when studying particular structural features, has driven research into halogenation[18–24] and the methylation[25,26] at various Im positions. To the best of our knowledge, in the realm of 1,3-dialkyl-Im-based salts, several molecules with halogen substitutions at the 2-, 4- or 5- carbon positions were reported,[27] but trisubstituted derivatives are the less abundant. The only account of 1,3-dialkyl-2,4,5-trifluoro-Im-based salts containing an iodine counteranion ($[C_nC_1F_3Im][I]$) was reported in a patent, but it provided very limited characterization.[28] However, there are indeed two reports of 1,3-$R_2$-4,5-difluoro-Im triflate with *R* being 2,6-diisopropylphenyl, 2,4,6-trimethylphenyl and cyclohexyl groups[29,30], following a similar strategy to previous Cl and Br substitution of 4- and 5- positions.[31,32]

## 2. Detailed discussion on the analyses of aggregation

The PNPP in the *S(q)* suggests a mesophase segregation in most of the studied [C$_n$C$_1$F$_3$Im][Cl] ILs (Figure 1A). The analyses of the aggregation patterns presented in Figure 1G provides further insights into these coexisting sub-phases: the polar network (cation and anion polar centres) and the nonpolar subdomain (cation alkyl side chains from C2 on). First, the polar network (continuous lines, Figure 1G) forms a single aggregate gathering nearly all the ion pairs present in each case studied, and the effect of larger alkyl lengths is limited to a slight broadening of this distribution. On the other hand, the alkyl chain length plays a critical role in forming a continuous nonpolar phase (dotted lines, Figure 1G), since: (i) the short alkyl chain in [C$_2$C$_1$F$_3$Im][Cl] has only about 1.44 analogous chains in close contact (circles, Figure 1D), insufficient to connect all analogous groups, and thus the simulation contains a large number of small, isolated nonpolar aggregates (Figure 1G); (ii) the alkyl chains in [C$_4$C$_1$F$_3$Im][Cl] are surrounded by approximately 3.15 akin tails (circles, Figure 1D) resulting in an almost continuous nonpolar sub-phase encompassing *ca*. 97% (accumulated probability) of the alkyl chains (Figure 1G); and (iii) for longer alkyl chains, the system forms a single, continuous nonpolar aggregate (Figure 1G). The progression of $N_i$ values for alkyl chains in the [C$_n$C$_1$F$_3$Im][Cl] series (circles, Figure 1D) is similar to trends observed in [C$_n$C$_1$Im][NTf$_2$] [33,34] and [K][C$_n$C$_1$Cp].[10,11] It must be noticed that the analysis of the polar network continuity (Figure 1G) has been performed considering all the anions in the first solvation shell of the cation (second peak in the cation-anion *g(r)*). This approach accounts for anions from both (i) the chain of stacked ions to which the studied cation belongs and (ii) inter-chain connectivity. If the analysis focuses exclusively on the continuity of the polar network formed only by threads of stacked anions and cations (first peak in the cation-anion *g(r)*), as in previous works,[10,11] more fragmented but still continuous distributions are obtained for the [C$_n$C$_1$F$_3$Im][Cl] series (Figure S11A).

The comparison between the more continuous distributions of the polar chains in [C$_n$C$_1$F$_3$Im][Cl] (Figure S11A) and those in [K][C$_4$C$_1$Cp][10,11] reveal the more branched nature of the stacked cations and anions chains in the former. Unless stated otherwise, this study considers the continuity of the polar domain as the network formed by the cation and all the anions in its first solvation shell (second peak in the cation-anion *g(r)*). However, the corresponding analyses considering only stacked anion and cation chains (first peak in the cation-anion *g(r)*) is available in Figure S11.

## 3. Supplementary simulations data

**Table S1:** Details of the molecular dynamics (MD) simulations performed at 400 K and 1 bar: ion pair molecular mass (IpMM), number of ionic pairs ($n_{box}$), box edge length ($l$) and simulated density ($\rho_{sim}$).

| Ionic Liquid | IpMM | $n_{box}$ | $l$ (Å) | $\rho_{sim}$ |
|---|---|---|---|---|
| $[C_2C_1F_3Im][Cl]$ | 200.6 | 700 | 56.48 | 1.294 |
| $[C_4C_1F_3Im][Cl]$ | 228.6 | 700 | 60.71 | 1.188 |
| $[C_6C_1F_3Im][Cl]$ | 256.7 | 700 | 64.48 | 1.113 |
| $[C_8C_1F_3Im][Cl]$ | 284.8 | 700 | 67.77 | 1.063 |
| $[C_{10}C_1F_3Im][Cl]$ | 312.8 | 700 | 70.73 | 1.028 |
| $[C_2C_1F_3Im][Br]$ | 245.0 | 700 | 57.14 | 1.526 |
| $[C_4C_1F_3Im][Br]$ | 273.1 | 700 | 61.23 | 1.383 |
| $[C_6C_1F_3Im][Br]$ | 301.2 | 700 | 64.93 | 1.279 |
| $[C_8C_1F_3Im][Br]$ | 329.2 | 700 | 68.49 | 1.191 |
| $[C_{10}C_1F_3Im][Br]$ | 357.3 | 700 | 71.15 | 1.153 |
| $[C_2C_1F_3Im][I]$ | 292.0 | 700 | 58.09 | 1.732 |
| $[C_4C_1F_3Im][I]$ | 320.1 | 700 | 62.03 | 1.559 |
| $[C_6C_1F_3Im][I]$ | 348.2 | 700 | 65.67 | 1.429 |
| $[C_8C_1F_3Im][I]$ | 376.2 | 700 | 68.87 | 1.339 |
| $[C_{10}C_1F_3Im][I]$ | 404.3 | 700 | 71.75 | 1.272 |
| $[C_2C_2F_3Im][Cl]$ | 215.6 | 700 | 58.53 | 1.250 |
| $[C_4C_4F_3Im][Cl]$ | 271.7 | 700 | 66.07 | 1.095 |
| $[C_6C_6F_3Im][Cl]$ | 327.8 | 700 | 72.23 | 1.011 |
| $[C_8C_8F_3Im][Cl]$ | 383.9 | 700 | 77.37 | 0.964 |
| $[C_{10}C_{10}F_3Im][Cl]$ | 440.1 | 700 | 81.82 | 0.934 |

**Table S2:** optimized *ab initio* (*cis* and *gauche*) structures for $[C_nC_1F_3Im]^+$ with n being 1, 2, 3 and 4 (MP2 theory level using cc-pVDZ and cc-pVTZ(-f) basis sets for the initial geometrical optimization and Single Point plus Population analysis, respectively):

| $[C_1C_1F_3Im]^+$ | | | | $[C_2C_1F_3Im]^+$ (configuration 1, TS) | | | | $[C_2C_1F_3Im]^+$ (configuration 2) | | | |
|---|---|---|---|---|---|---|---|---|---|---|---|
| Energy | -601.9262936 | Hartree | | Energy | -641.1511272 | Hartree | | Energy | -641.15475 | Hartree | |
| Imaginary freq. | None | | | Imaginary freq. | 1 (-35.5647) | | | Imaginary freq. | None | | |
| Atoms | Cartesian coordinates | | | Atoms | Cartesian coordinates | | | Atoms | Cartesian coordinates | | |
| C | 0.686 | -1.000 | 0.000 | C | 1.433 | 0.585 | 0.000 | C | 1.133 | 0.911 | 0.034 |
| C | -0.686 | -1.001 | 0.000 | C | 0.240 | 1.258 | 0.000 | C | -0.210 | 1.104 | -0.170 |
| N | -1.102 | 0.327 | 0.000 | N | -0.785 | 0.313 | 0.000 | N | -0.800 | -0.149 | -0.291 |
| N | 1.102 | 0.327 | 0.000 | N | 1.138 | -0.773 | 0.000 | N | 1.359 | -0.462 | 0.044 |
| C | 2.506 | 0.785 | 0.000 | C | 2.132 | -1.863 | 0.000 | C | 2.670 | -1.113 | 0.227 |
| H | 3.002 | 0.404 | -0.903 | H | 2.751 | -1.778 | 0.903 | H | 3.076 | -0.825 | 1.205 |
| H | 2.501 | 1.882 | 0.000 | H | 1.586 | -2.815 | 0.000 | H | 2.514 | -2.198 | 0.183 |
| H | 3.001 | 0.405 | 0.904 | H | 2.751 | -1.778 | -0.903 | H | 3.341 | -0.791 | -0.581 |
| C | 0.000 | 1.088 | 0.000 | C | -2.230 | 0.704 | -0.001 | C | -2.255 | -0.408 | -0.464 |
| F | -0.001 | 2.390 | 0.000 | H | -2.365 | 1.333 | 0.892 | H | -2.593 | 0.277 | -1.255 |
| F | 1.570 | -1.966 | 0.000 | H | -2.366 | 1.332 | -0.894 | H | -2.336 | -1.439 | -0.838 |
| F | -1.570 | -1.967 | 0.000 | C | -0.198 | -0.893 | 0.000 | C | 0.174 | -1.057 | -0.150 |
| C | -2.506 | 0.784 | 0.000 | F | -0.808 | -2.045 | 0.000 | F | -0.006 | -2.346 | -0.198 |
| H | -3.002 | 0.404 | -0.903 | F | 2.679 | 0.989 | 0.000 | F | 2.131 | 1.743 | 0.199 |
| H | -3.002 | 0.404 | 0.903 | F | -0.050 | 2.536 | 0.000 | F | -0.938 | 2.190 | -0.268 |
| H | -2.501 | 1.881 | 0.000 | C | -3.187 | -0.478 | 0.001 | C | -3.008 | -0.200 | 0.844 |
| | | | | H | -3.074 | -1.102 | -0.898 | H | -2.649 | -0.891 | 1.623 |
| | | | | H | -3.074 | -1.101 | 0.900 | H | -2.907 | 0.837 | 1.200 |
| | | | | H | -4.208 | -0.066 | 0.001 | H | -4.077 | -0.400 | 0.671 |

| $[C_3C_1F_3Im]^+$ (configuration 1, TS) | | | | $[C_3C_1F_3Im]^+$ (configuration 2) | | | | $[C_4C_1F_3Im]^+$ (configuration 1, TS) | | | | $[C_4C_1F_3Im]^+$ (configuration 2) | | | |
|---|---|---|---|---|---|---|---|---|---|---|---|---|---|---|---|
| Energy | -680.3744134 | Hartree | | Energy | -680.378386 | Hartree | | Energy | -719.5970868 | Hartree | | Energy | -719.6010067 | Hartree | |
| Imaginary freq. | 1 (-31.3468) | | | Imaginary freq. | None | | | Imaginary freq. | 1 (-26.2015) | | | Imaginary freq. | None | | |
| Atoms | Cartesian coordinates | | | Atoms | Cartesian coordinates | | | Atoms | Cartesian coordinates | | | Atoms | Cartesian coordinates | | |
| C | -1.839 | 0.601 | 0.000 | C | 1.598 | 0.850 | 0.073 | C | -2.327 | 0.460 | 0.000 | C | 1.988 | 0.857 | 0.154 |
| C | -0.636 | 1.256 | 0.000 | C | 0.286 | 1.140 | -0.205 | C | -1.201 | 1.240 | 0.000 | C | 0.716 | 1.136 | -0.275 |
| N | 0.375 | 0.296 | 0.000 | N | -0.383 | -0.067 | -0.377 | N | -0.093 | 0.395 | 0.000 | N | 0.080 | -0.076 | -0.520 |
| N | -1.565 | -0.760 | 0.000 | N | 1.725 | -0.536 | 0.077 | N | -1.908 | -0.864 | 0.000 | N | 2.124 | -0.528 | 0.179 |
| C | -2.575 | -1.836 | 0.000 | C | 2.974 | -1.282 | 0.324 | C | -2.795 | -2.043 | 0.000 | C | 3.341 | -1.263 | 0.573 |
| H | -3.193 | -1.742 | -0.903 | H | 3.343 | -1.032 | 1.327 | H | -3.420 | -2.016 | -0.903 | H | 3.589 | -1.007 | 1.611 |
| H | -2.043 | -2.796 | -0.001 | H | 2.743 | -2.352 | 0.257 | H | -2.163 | -2.939 | -0.001 | H | 3.127 | -2.335 | 0.485 |
| H | -3.193 | -1.742 | 0.903 | H | 3.711 | -1.001 | -0.441 | H | -3.419 | -2.017 | 0.903 | H | 4.160 | -0.981 | -0.102 |
| C | 1.825 | 0.663 | 0.001 | C | -1.842 | -0.219 | -0.620 | C | 1.311 | 0.916 | 0.001 | C | -1.340 | -0.239 | -0.927 |
| H | 1.973 | 1.291 | -0.892 | H | -2.103 | 0.519 | -1.394 | H | 1.390 | 1.555 | -0.893 | H | -1.515 | 0.491 | -1.732 |
| H | 1.974 | 1.289 | 0.895 | H | -1.979 | -1.227 | -1.040 | H | 1.390 | 1.554 | 0.894 | H | -1.423 | -1.251 | -1.351 |
| C | 2.778 | -0.527 | -0.001 | C | -2.645 | -0.013 | 0.663 | C | 2.385 | -0.165 | 0.000 | C | -2.286 | -0.030 | 0.253 |
| H | 2.602 | -1.153 | 0.890 | H | -2.315 | -0.750 | 1.416 | H | 2.280 | -0.808 | 0.891 | H | -2.043 | -0.759 | 1.048 |
| H | 2.602 | -1.151 | -0.892 | H | -2.433 | 0.993 | 1.064 | H | 2.280 | -0.807 | -0.892 | H | -2.130 | 0.982 | 0.670 |
| C | -0.231 | -0.901 | 0.000 | C | 0.514 | -1.043 | -0.192 | C | 3.773 | 0.491 | 0.000 | C | -3.748 | -0.194 | -0.179 |
| F | 0.360 | -2.063 | 0.001 | F | 0.246 | -2.316 | -0.267 | H | 3.867 | 1.143 | -0.887 | H | -3.972 | 0.529 | -0.985 |
| F | -3.079 | 1.025 | -0.001 | F | 2.642 | 1.607 | 0.306 | H | 3.868 | 1.143 | 0.887 | H | -3.890 | -1.203 | -0.608 |
| F | -0.328 | 2.530 | 0.000 | F | -0.357 | 2.276 | -0.328 | C | 4.891 | -0.554 | -0.001 | C | -4.712 | 0.015 | 0.991 |
| C | 4.221 | -0.010 | -0.001 | C | -4.143 | -0.168 | 0.385 | H | 4.829 | -1.198 | -0.894 | H | -4.604 | 1.027 | 1.415 |
| H | 4.925 | -0.856 | -0.002 | H | -4.719 | -0.020 | 1.311 | H | 5.878 | -0.068 | -0.001 | H | -5.756 | -0.105 | 0.664 |
| H | 4.425 | 0.602 | -0.894 | H | -4.489 | 0.575 | -0.353 | H | 4.830 | -1.198 | 0.892 | H | -4.522 | -0.716 | 1.794 |
| H | 4.426 | 0.600 | 0.894 | H | -4.375 | -1.175 | -0.001 | C | -0.566 | -0.860 | 0.000 | C | 0.956 | -1.045 | -0.227 |
| | | | | | | | | F | 0.146 | -1.952 | 0.000 | F | 0.708 | -2.320 | -0.327 |
| | | | | | | | | F | -3.605 | 0.748 | 0.000 | F | 2.993 | 1.623 | 0.504 |
| | | | | | | | | F | -1.033 | 2.540 | 0.000 | F | 0.084 | 2.267 | -0.478 |

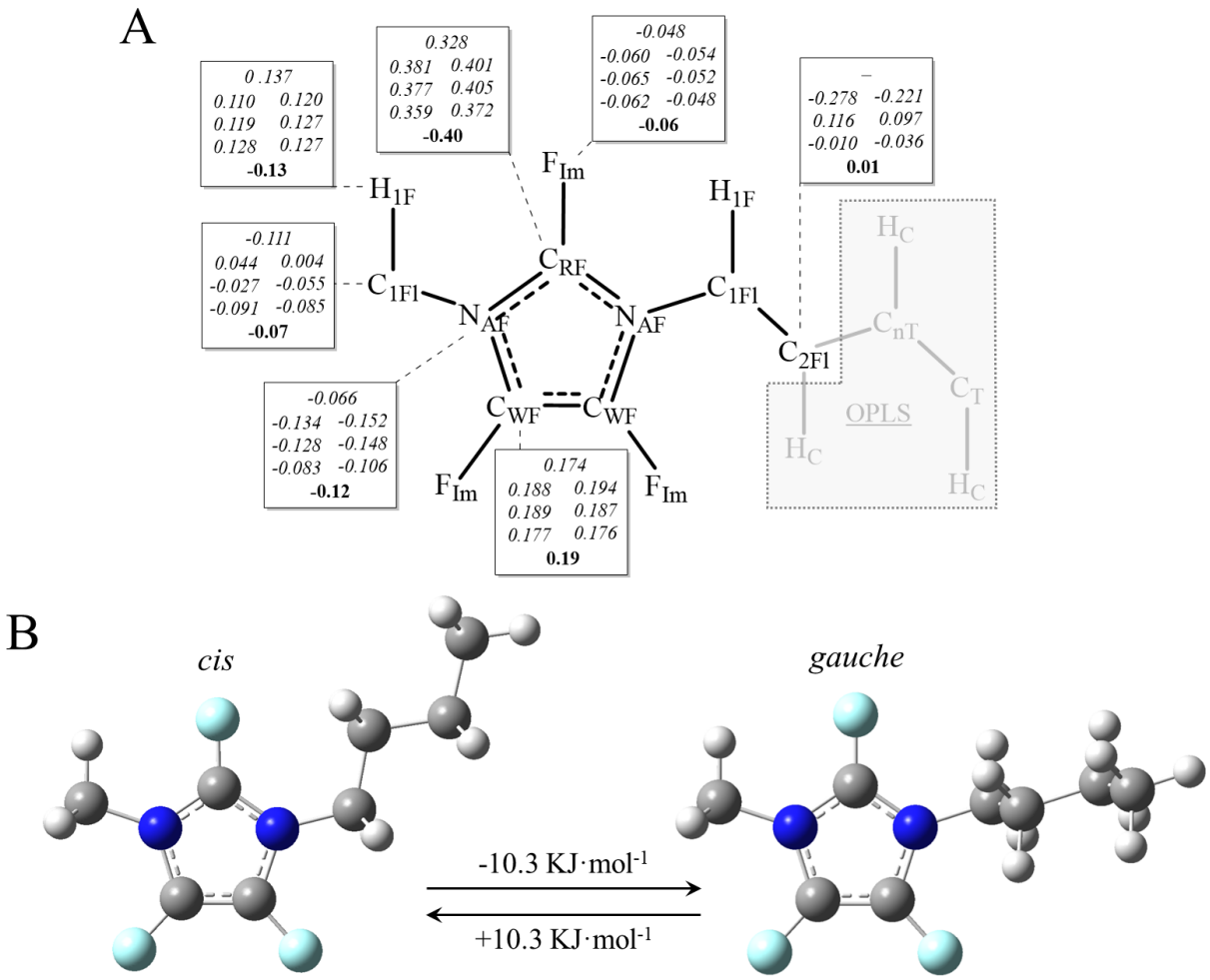


**Figure S1:** Results from the *ab initio* calculations performed to determine the atomic charges for the Force Field. The calculations were performed at the MP2 theoretical level with the cc-pVTZ(-f) basis set, using the ChelpG electrostatic surface potential methodology. (A) The mean atomic charges for each atom type in 1-alkyl-3-methyl-2,4,5-fluoro-Imidazolium ($[C_nC_1F_3Im]^+$) are shown in italics for alkyl chain lengths from $n$=1 (top number in italics) to $n$=4 (bottom numbers in italics), for the two main alkyl conformers (*cis* and *gauche*, in the left and right columns of values in italics, respectively). The numbers highlighted in bold are the atomic charges selected for each case, based on both the transferability of the atom and the reference-weighted *ab initio* values (see simulation details). Atoms within the grey box (representing the alkyl chain) were treated as OPLS.[36] (B) Optimized structures for the two main alkyl conformers used for calculating the atomic charges of $[C_4C_1F_3Im]^+$. These conformers correspond presented in (A), with the left conformer matching the left column and the right conformer matching the right column.

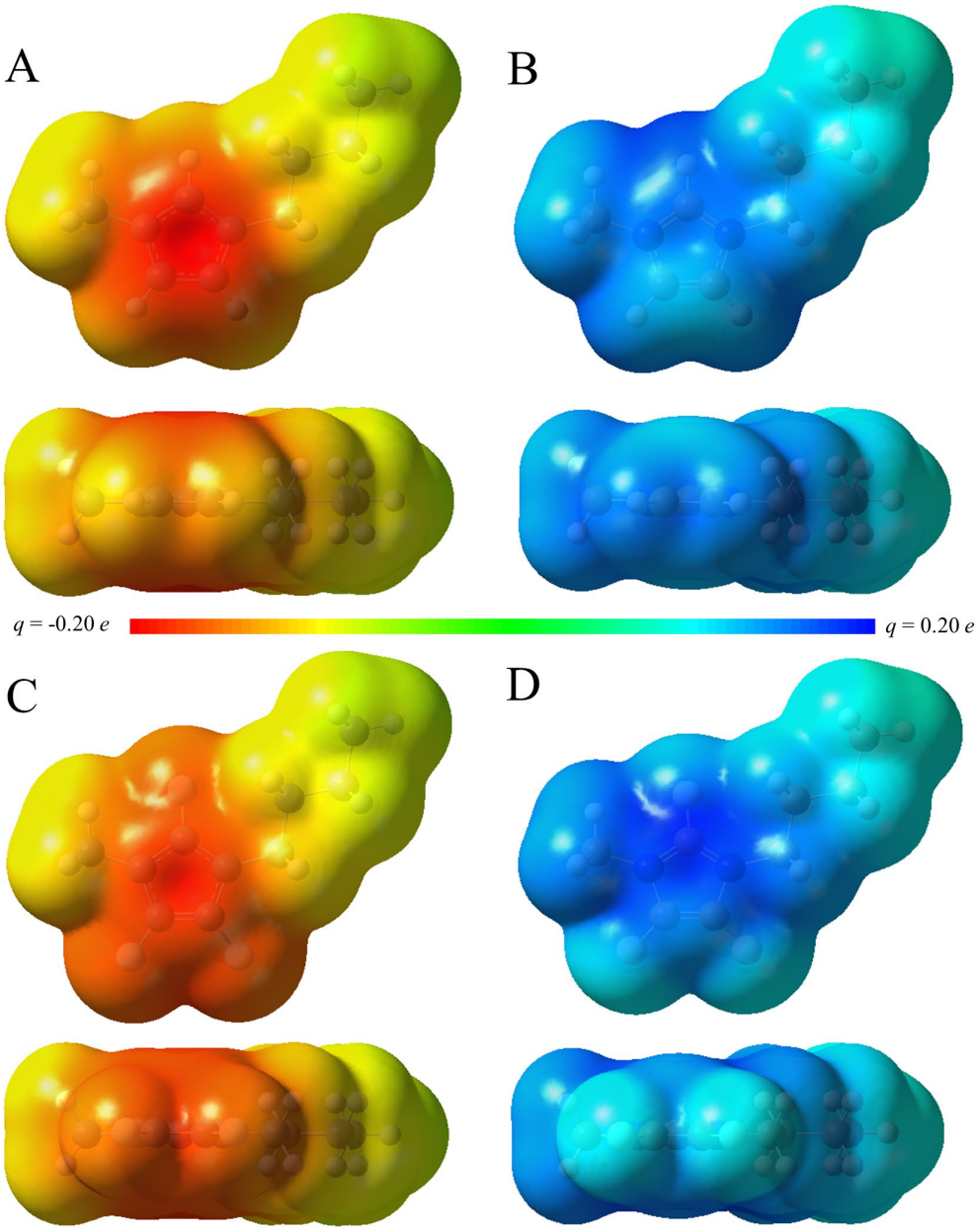


**Figure S2:** Electrostatic surface potential (ESP) for: (A) $[C_4C_1Cp]^-$, (B) $[C_4C_1Im]^+$, (C) $[C_4C_1F_3Cp]^-$, and (D) $[C_4C_1F_3Im]^+$. These ESPs were calculated using the ChelpG methodology at the MP2 theoretical level with the cc-pVTZ(-f) basis set, following previous geometric optimization. The *cis* conformers (Figure S1) are presented to ease visualization.

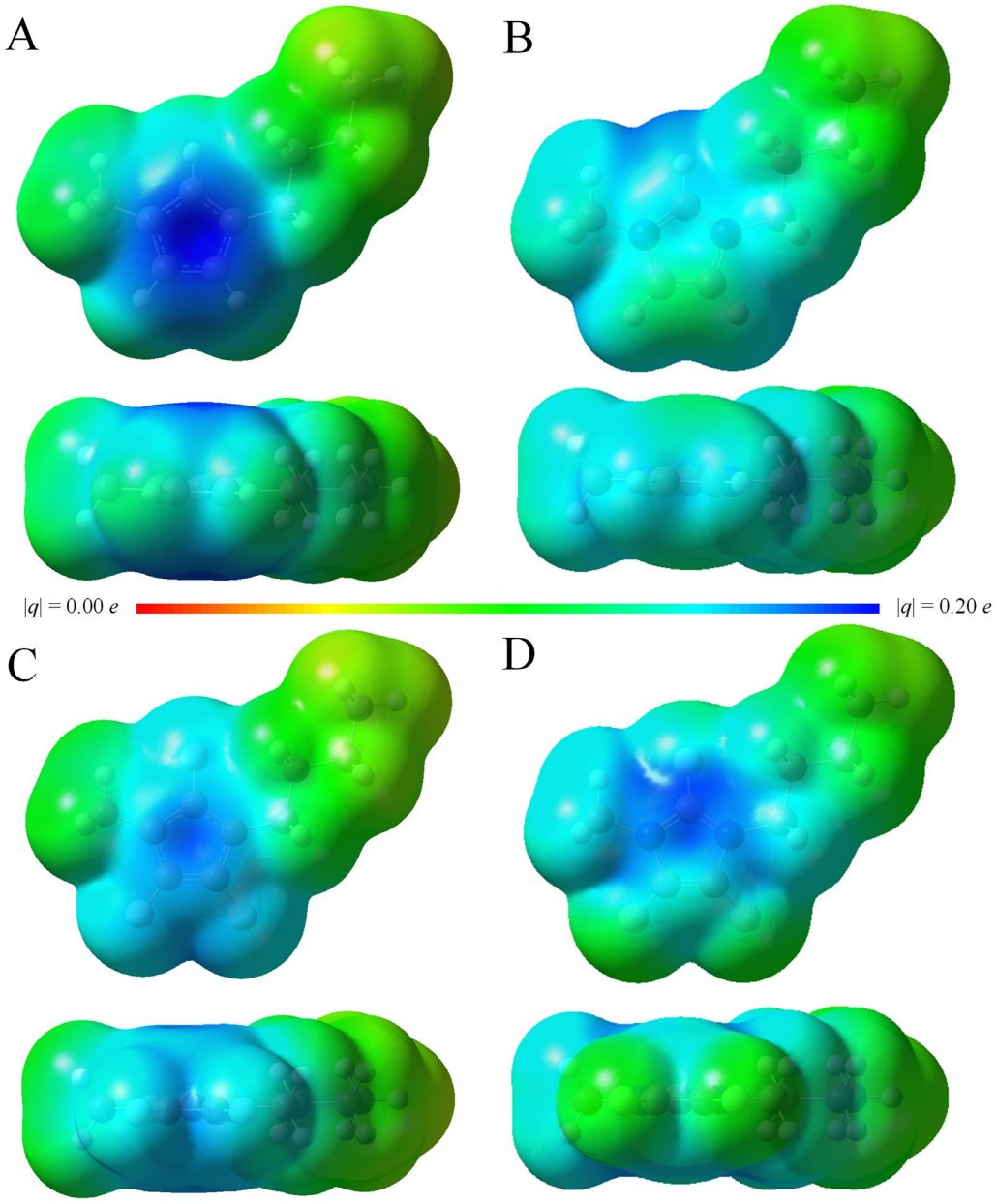


**Figure S3:** Absolute values of the electrostatic surface potential (ESP) for: (A) $[C_4C_1Cp]^-$, (B) $[C_4C_1Im]^+$, (C) $[C_4C_1F_3Cp]^-$ and (D) $[C_4C_1F_3Im]^+$. Data reconverted from Figure S2.

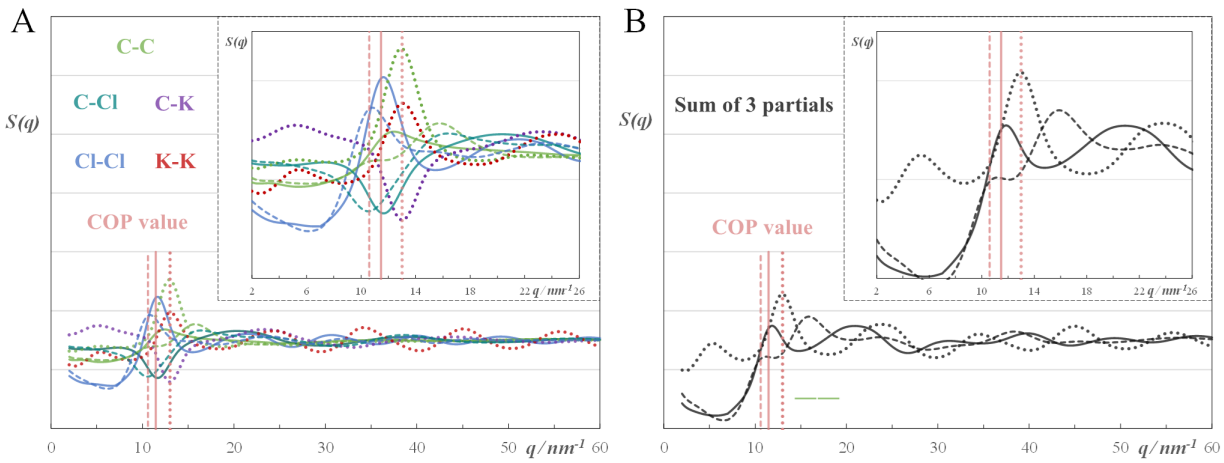


**Figure S4:** Atomic partial structure factors (*S(q)*s) for $[C_4C_1F_3Im][Cl]$ (continuous (—) lines), $[K][C_4C_1Cp]$ (dotted (⋯) lines), and $[C_4C_1Im][Cl]$ (dashed (- - -) lines): (A) three main atomic partial *S(q)* suggesting ion alternation: Carbon-Carbon (C-C), Carbon-Anion or Carbon-Cation (C-Cl and C-K) and Anion-Anion or Cation-Cation (Cl-Cl and K-K); (B) The sum of the 3 partials from (A). The vertical pink line illustrates the location of the charge-ordering peak (COP), determined by gaussian deconvolution of the complete *S(q)*. Data for $[K][C_4C_1Cp]$ and $[C_4C_1Im][Cl]$ were obtained from previous works.[10,11]

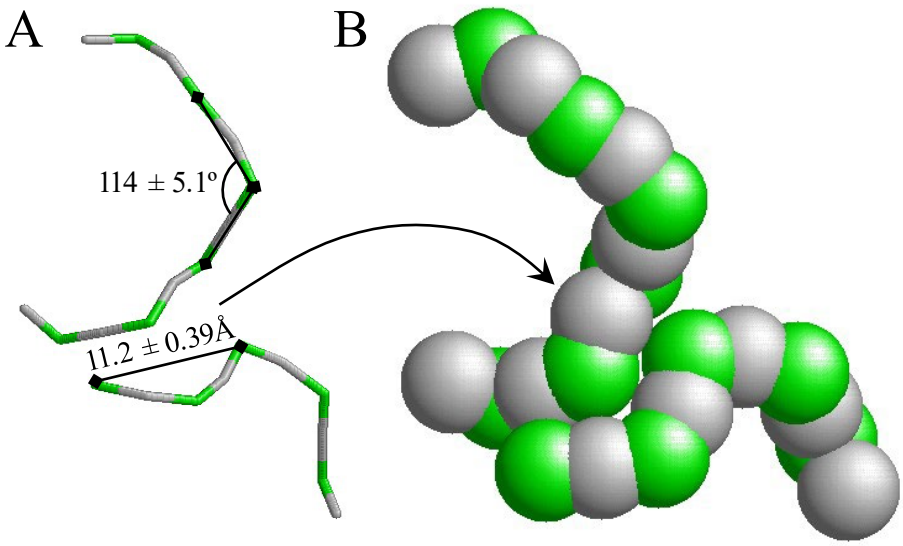


**Figure S5:** Snapshot of randomly selected chains from the $[C_4C_1F_3Im][Cl]$ simulation box: green codifies the anion and grey the cation core mass centre. Each of the two chains contains 22 atoms (note that the cation core mass centre is treated here as an atom). (A) Displays the atoms connected by bars to facilitate visualization of atomic connectivity, including the mean and sample standard deviation values for the distance and angle formed by 2 anions within the same chain, separated by another anion. (B) Shows the space-filling representation of the same chains, which provides a clearer visualization of the inter-chain interactions.

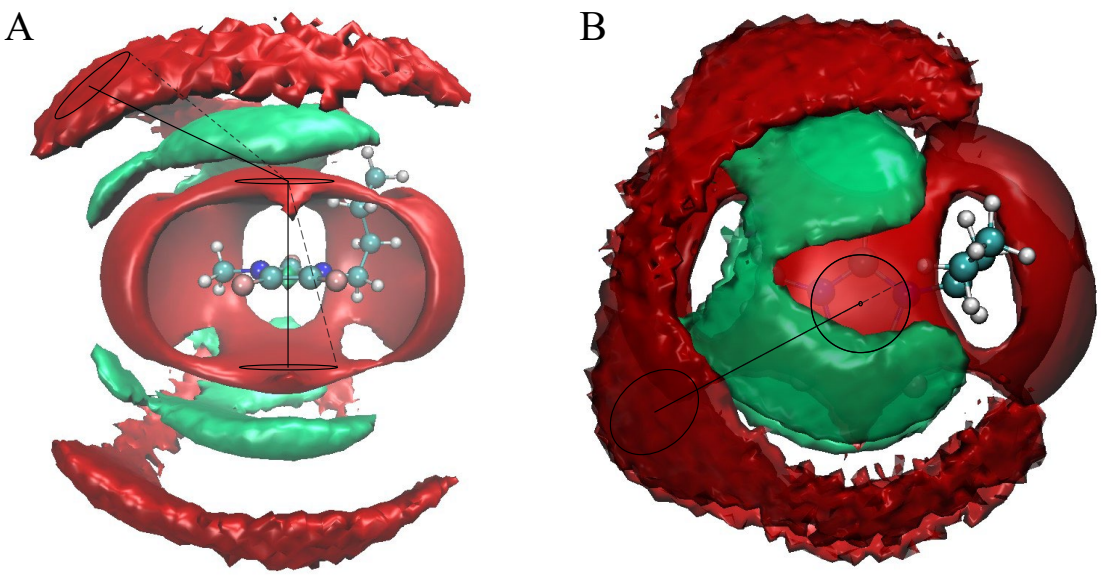


**Figure S6:** Spatial distribution functions (*sdf*s) for the location of the anion (red cloud) and cation mass centre (cyan cloud) around the cation in $[C_4C_1F_3Im][Cl]$: (A) axial and (B) zenithal perspectives. The *sdf*s cut-offs are set at (i) 2% of the maximum distance for the anion (red cloud) and (ii) 0.1% for the cation mass centre (cyan cloud). The *sdf* for the cation mass centre includes the mass centre of the probe (cation) molecule, visible as small rhomboid cloud within the core in (A), which explains the small cut-off distance required to observe the first cations surrounding the examined cation. The black lines are visual guides, illustrating one of the reasons for part of the variability in the angle and distance calculated for 3 consecutive anions within the same chain (Figure S5).

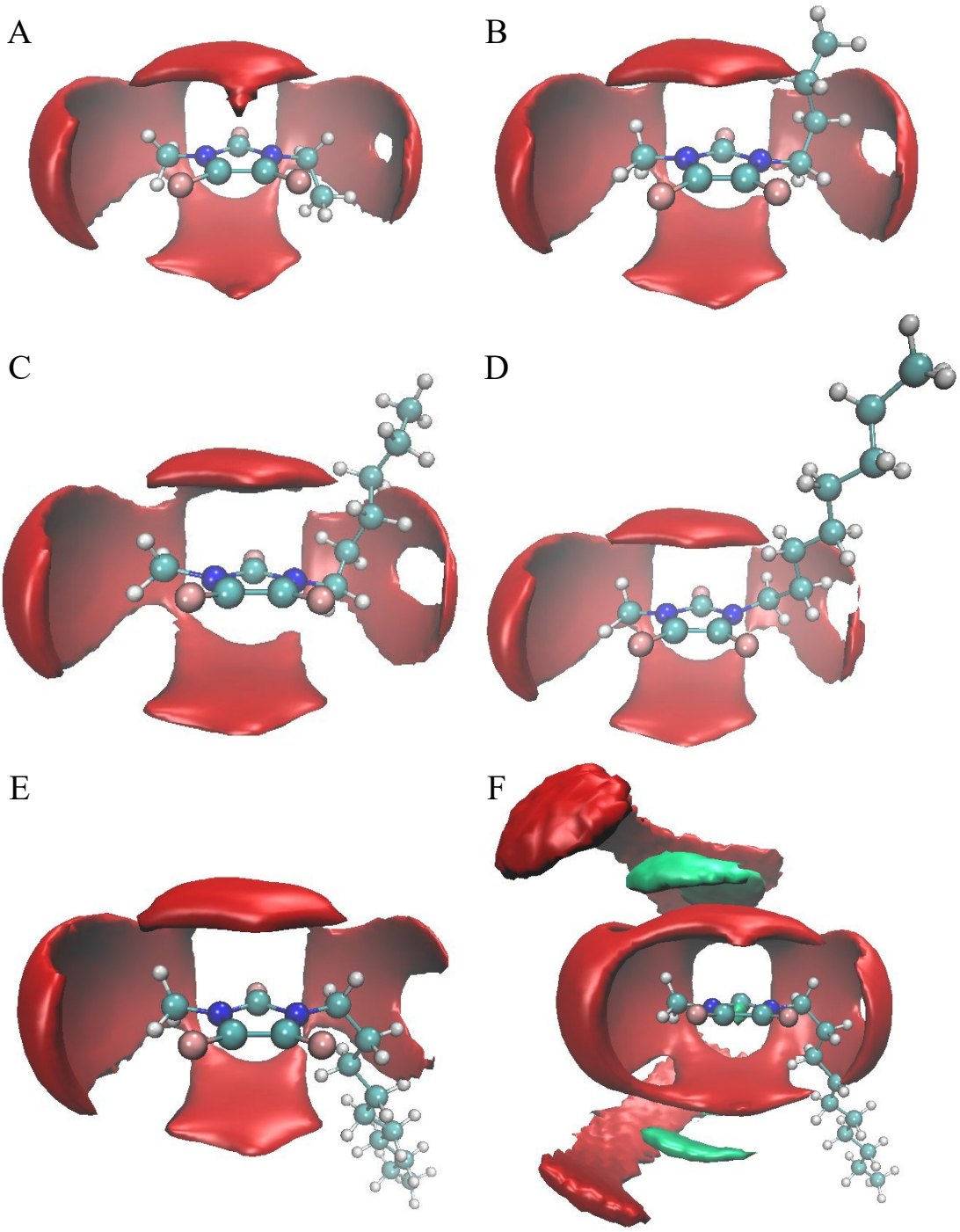


**Figure S7:** Spatial distribution functions (*sdf*s) showing the location of the anion (red cloud) around the cation in the $[C_nC_1F_3Im][Cl]$ series: (A) $[C_2C_1F_3Im][Cl]$, (B) $[C_4C_1F_3Im][Cl]$, (C) $[C_6C_1F_3Im][Cl]$, (D) $[C_8C_1F_3Im][Cl]$ and (E and F) $[C_{10}C_1F_3Im][Cl]$. For (A), (B), (C), (D) and (E), the *sdf*s cut-offs are set at ~~a~~ 4% of the maximum distance to display the complete first solvation shell of anions around the cations. In (F), the *sdf* cut-off is set at 2% of the maximum distance for the anion (red cloud), and 0.1% for the cation mass centre (cyan cloud) surrounding the cation. The *sdf* for the cation mass centre in (F) includes the mass centre of the probe molecule (cation), visible as a small rhomboid cloud within the core, which explains the smaller cut-off distance required to observe the first cations surrounding the examined cation.

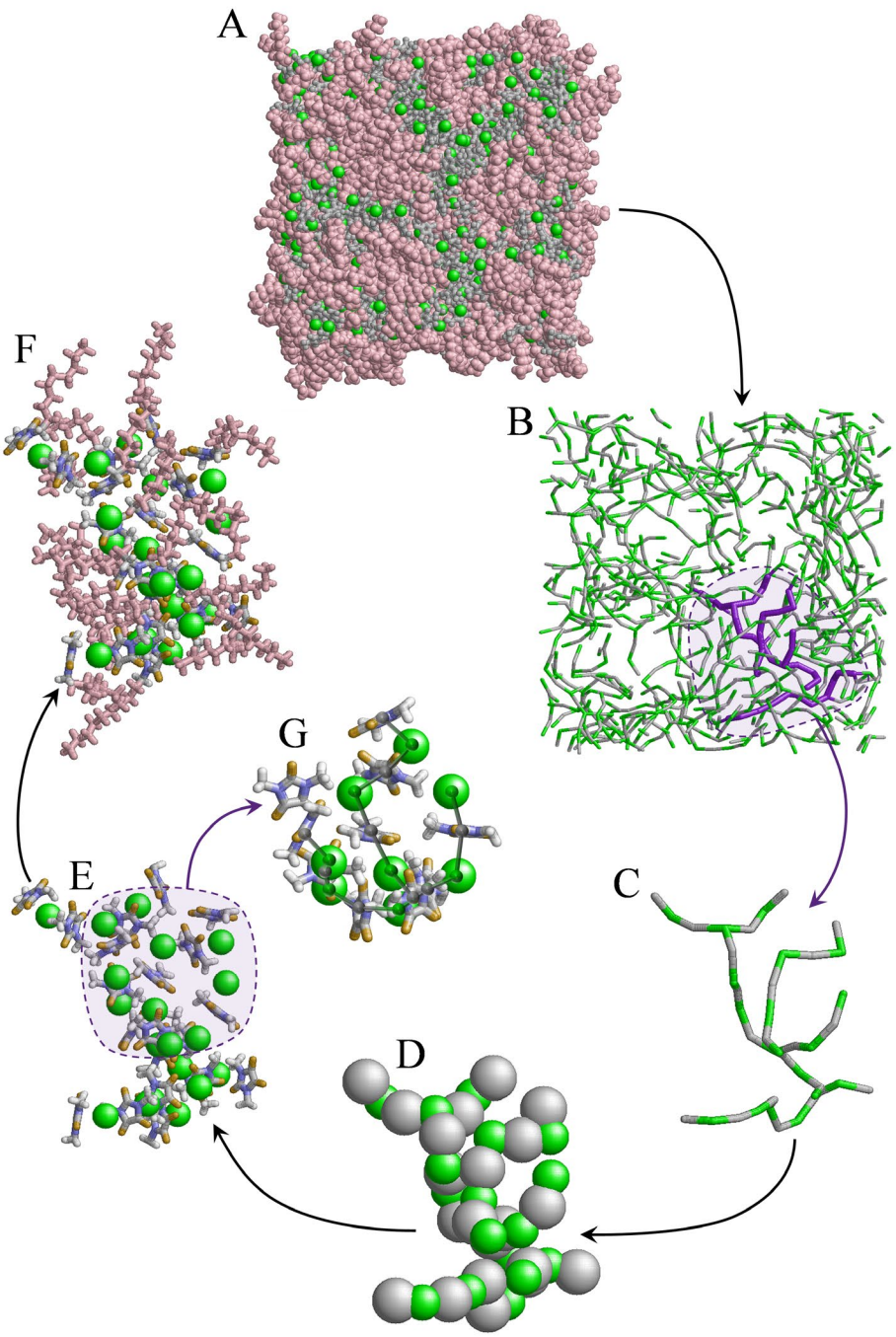


**Figure S8:** Snapshots of the final configuration for the $[C_{10}C_1F_3Im][Cl]$ simulations: (A) Full simulation box with atoms represented as spheres; (B) Bar representation of the polar network (consisting of the anion and the cation core mass centre) for the entire simulation box; (C) Zoomed-in view of a randomly selected region of the former polar network, highlighting closely interacting chains; (D) Spheres representation of the selected chains, showing direct contacts between chains; (E) Atomic representation of the selected chains, with the cation mass centre replaced by its constituent atoms; (F) Inclusion of the aliphatic chains from the cation in the selected chains; (G) Further magnification view of the selected section from (E). The colours code is: (i) Green – anion; (ii) Grey – carbon from the polar section of the cation and cation mass centre; (iii) Blue – nitrogen; (iv) Yellow – fluorine; (v) White – hydrogens from the polar section; and (vi) Pink – aliphatic chains. The lines in (G) are visual guides for illustrating the connectivity between the different chains.

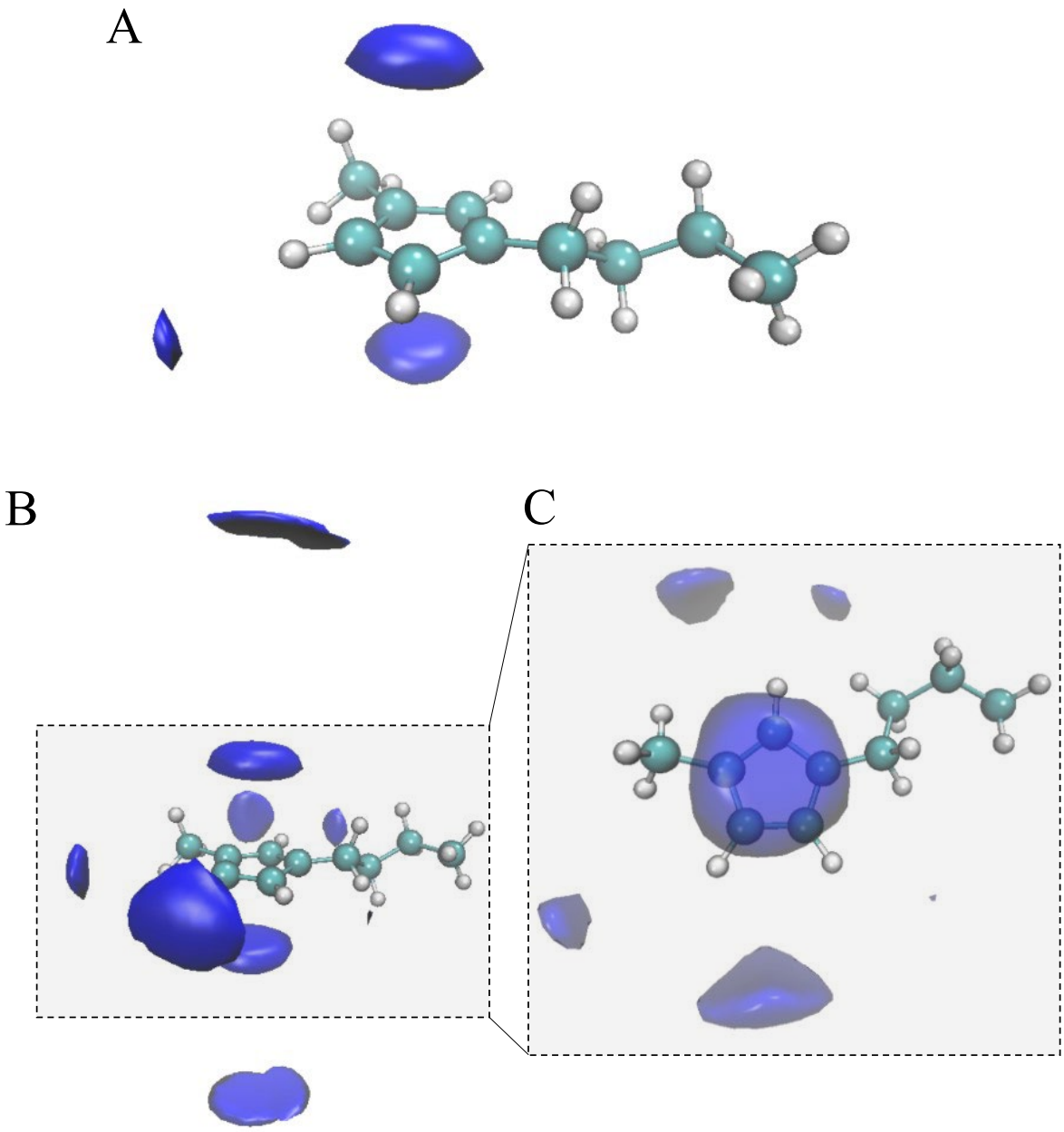


**Figure S9:** Spatial distribution functions (*sdf*s) for the location of the cation (blue cloud) around the anion in [K][$C_4C_1$Cp]. (A) The *sdf* cut-off set at 4% of the maximum distance, as in Figure S7A to S7E; (B) the *sdf* cut-off is set at 1.0% of the maximum distance to visualize how cations from other polar chains of stacked ions approach the Cp in the direction of the plane; (C) Provides a magnified view of the system shown in (B) with a different perspective, omitting the more distant clouds (second above and below) for clarity. These data were obtained by re-analysing simulations from *Cruz et al.* (2018 and 2019).[10,11]

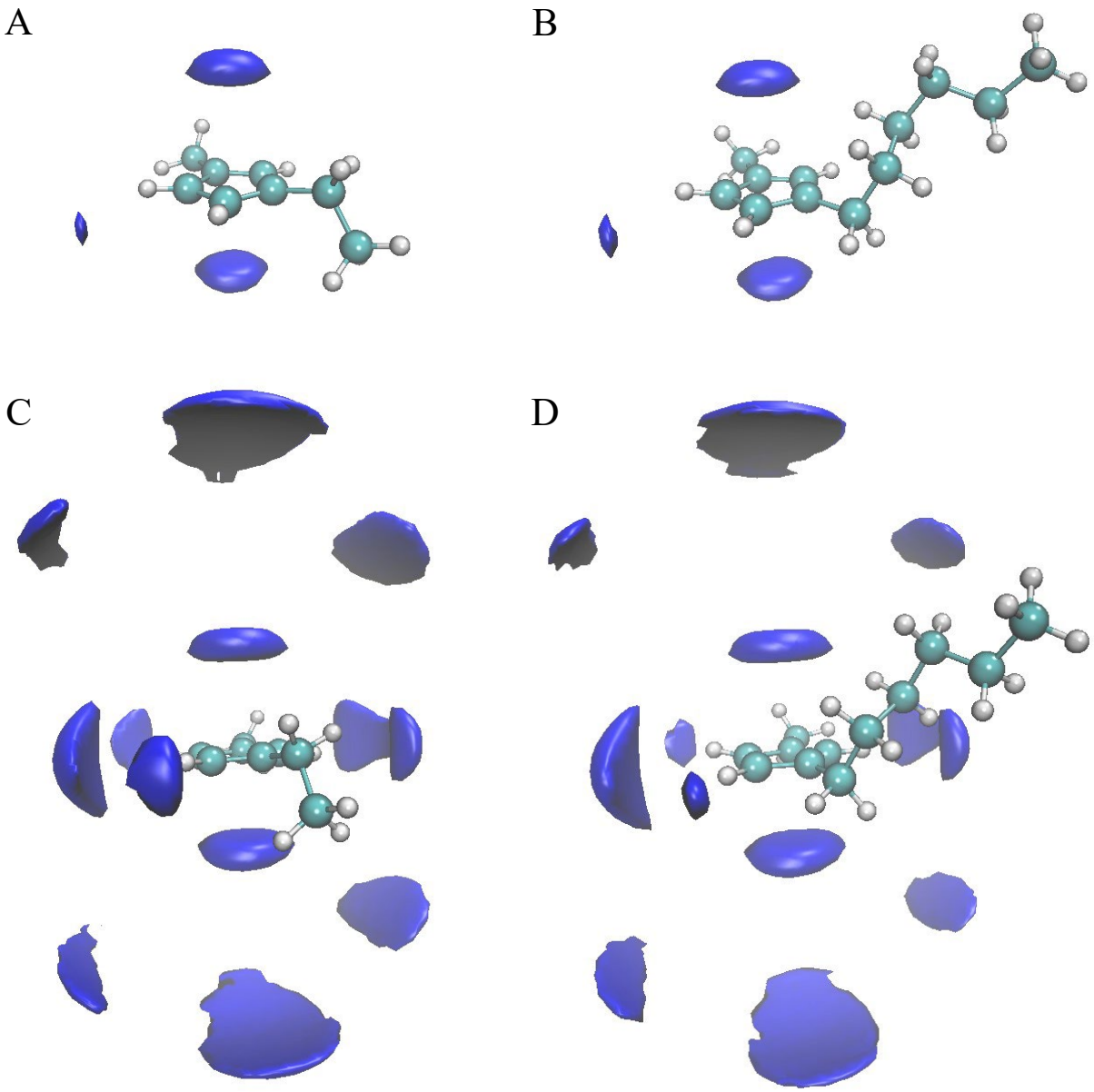


**Figure S10:** Spatial distribution functions (*sdf*s) for the location of the cation (blue cloud) around the anion in: (A and C) [K][$C_2C_1Cp$] and (B and D) [K][$C_6C_1Cp$]. In (A) and (B), the *sdf* cut-offs are set at 4% of the maximum distance, as in Figure S7A to S7E. In (C) and (D), the *sdf* cut-offs are set at 0.75% of the maximum distance to visualize the location of cations from other polar chains of stacked ions near the reference Cp, as in Figure 2B. These data were obtained by re-analysing simulations from *Cruz et al.* 2018 and 2019.[10,11]

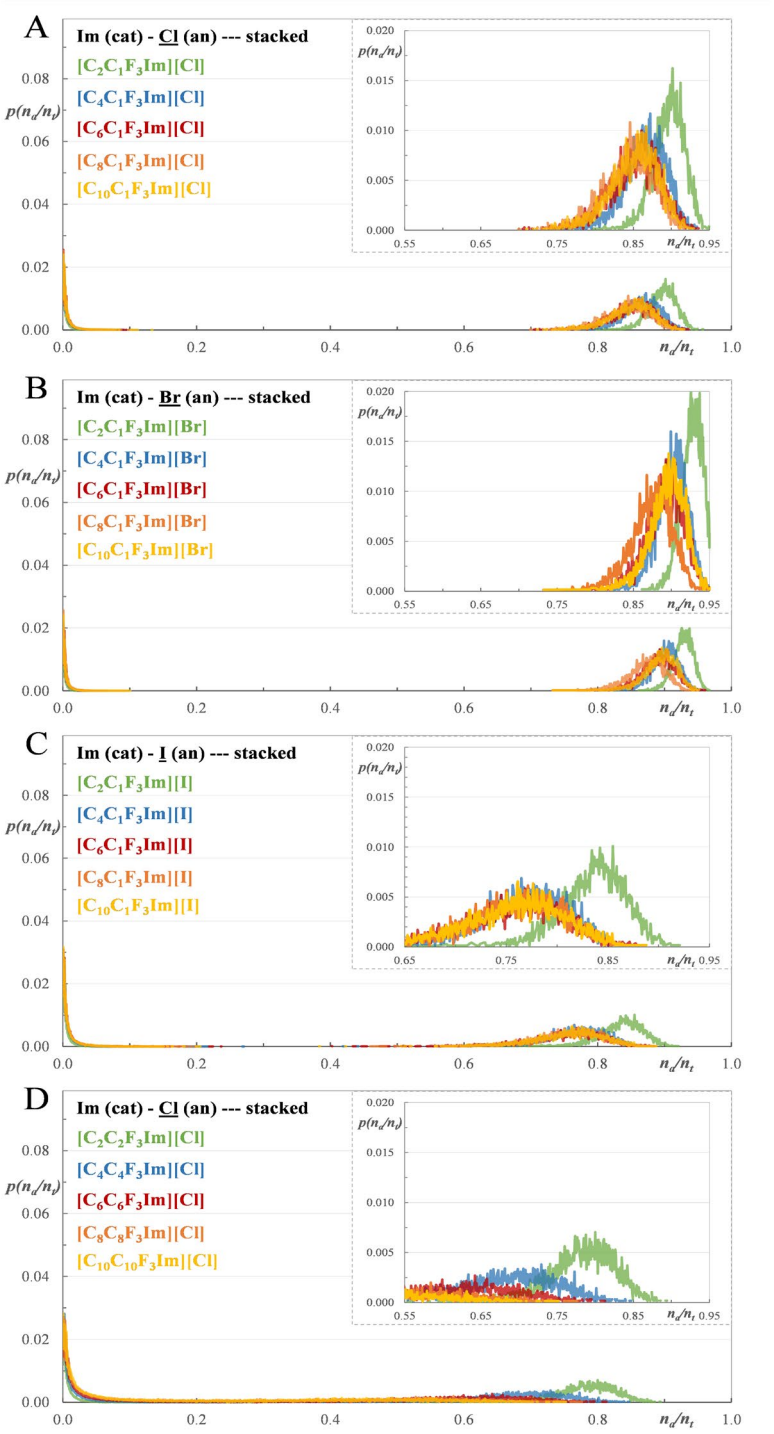


**Figure S11:** Number of aggregate sizes ($n_a$) relative to the number of ion pairs in the simulation box ($n_t$) and the probability of each relative aggregate size ($p(n_a/n_t)$): (A) [$C_nC_1F_3$Im][Cl] series; (B) [$C_nC_1F_3$Im][Br] series; (C) [$C_nC_1F_3$Im][I] series; and (D) [$C_nC_nF_3$Im][Cl] series.

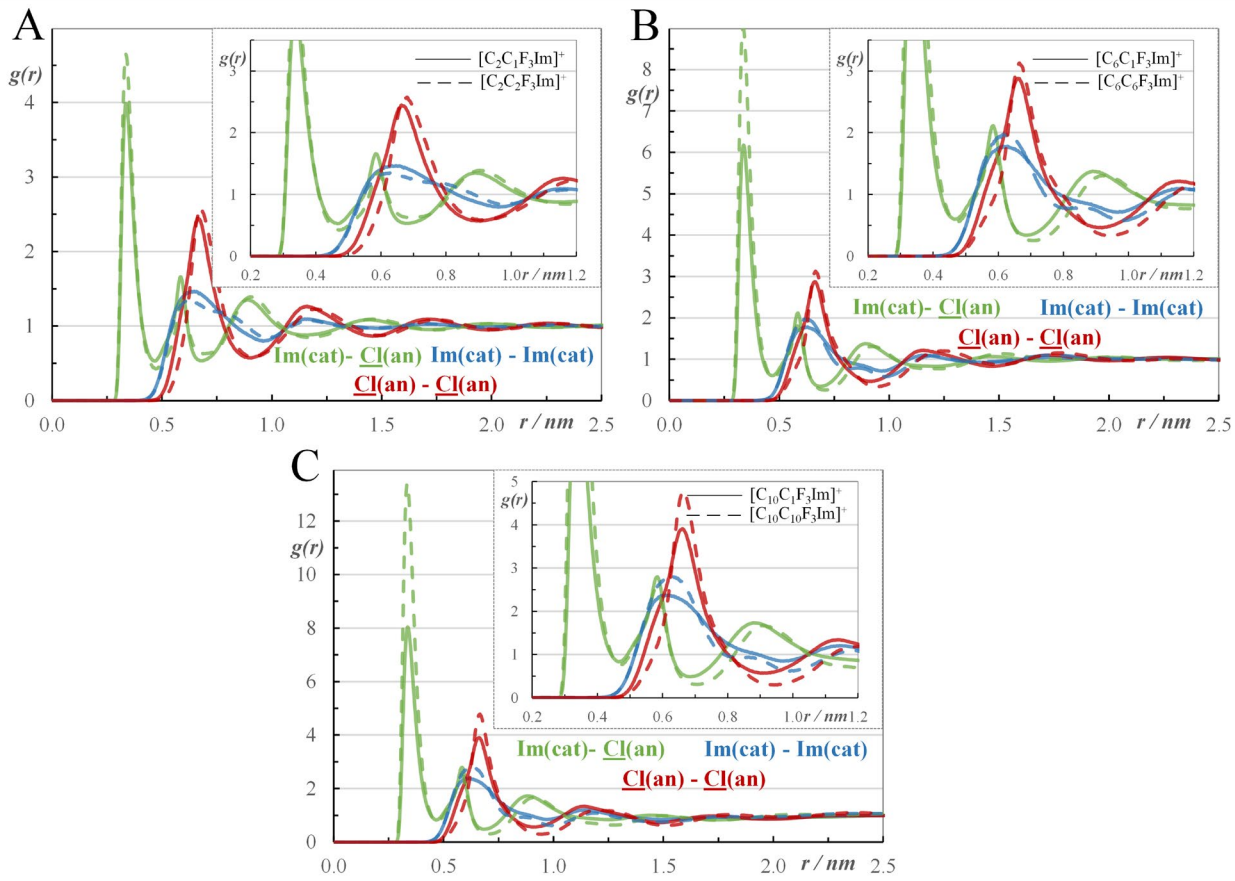


**Figure S12:** Radial distribution functions (*g(r)*s) between the mass centre of the imidazolium cation core (Im) and the anion (Cl): Im-Cl (green), Im-Im (blue) and Cl-Cl (red) for: (A) $[C_2C_1F_3Im][Cl]$ and $[C_2C_2F_3Im][Cl]$, (B) $[C_6C_1F_3Im][Cl]$ and $[C_6C_6F_3Im][Cl]$ and (C) $[C_{10}C_1F_3Im][Cl]$ and $[C_{10}C_{10}F_3Im][Cl]$. In these graphs, the continuous line (—)represents the $[C_nC_1F_3Im][Cl]$ series, while the dashed line (- - -) represents the $[C_nC_nF_3Im][Cl]$ series.

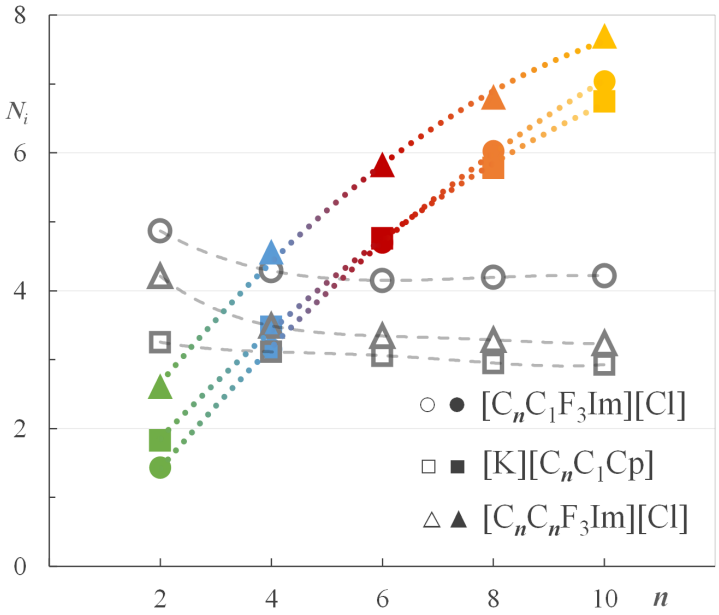


**Figure S13:** Number of direct contact neighbours ($N_i$) for the atomic ions in contact with the organic ion (open symbols) and connected aliphatic chains (closed symbols). Circles (○ ●) correspond to [$C_nC_1F_3Im$][Cl], squares (□ ■) to [K][$C_nC_1Cp$], and triangles (△ ▲) to [$C_nC_nF_3Im$][Cl]. The data compiled in this figure corresponds to Figures 3D, 4A, and 7B from the main document and is re-printed here to facilitate direct comparison.

## 4. References


1 F. Allouch, N. Dwadnia, N. V. Vologdin, Y. V. Svyaschenko, H. Cattey, M.-J. Penouilh, J. Roger, D. Naoufal, R. Ben Salem, N. Pirio and J.-C. Hierso, Converging and Diverging Synthetic Strategies to Tetradentate (N, N′)-Diaminomethyl,(P, P′)-Ferrocenyl Ligands: Influence of tert -Butyl Groups on Ferrocene Backbone Conformation, *Organometallics*, 2015, **34**, 5015–5028.

2 H. J. Bestmann and G. Wölfel, N,N-Bis(trimethylsilyl)aminomethylation of Grignard Compounds— A Versatile Amine Synthesis, *Angew. Chemie Int. Ed. English*, 1984, **23**, 53–53.

3 T. Nishinaga, D. Yamazaki, H. Stahr, A. Wakamiya and K. Komatsu, Synthesis, Structure, and Dynamic Behavior of Cyclopentadienyl-Lithium, -Sodium, and -Potassium Annelated with Bicyclo[2.2.2]octene Units: A Systematic Study on Site Exchange of Alkali Metals on a Cyclopentadienyl Ring in Tetrahydrofuran, *J. Am. Chem. Soc.*, 2003, **125**, 7324–7335.

4 G. Rabe, H. W. Roesky, D. Stalke, F. Pauer and G. M. Sheldrick, The preparation and crystal structures of sodium and potassium pentamethylcyclopentadienyl pyridine solvates, *J. Organomet. Chem.*, 1991, **403**, 11–19.

5 R. Lengacher, H. Braband, J. Csucker and R. Alberto, Convenient Cyclopentadiene Modifications for Building Versatile (Radio-)Metal Cyclopentadienyl Frameworks, *Eur. J. Inorg. Chem.*, 2021, **2021**, 1611–1614.

6 J. Lorberth, S.-H. Shin, S. Wocadlo and W. Massa, Pentabenzylcyclopentadienylpotassium ?? 3 THF, an Organopotassium Compound with“Piano Stool” Geometry, *Angew. Chemie Int. Ed. English*, 1989, **28**, 735–736.

7 C. Klein-Heßling and K. Sünkel, Synthesis and Spectroscopic Characterization of the Four Complete Series [(C 5 X n H 5-n )Fe(CO) 2 R] (X= Cl, Br; R= Me, Ph; n= 1–5). Molecular and Crystal Structures of [(C 5 X 5 )Fe(CO) 2 R], *ChemistrySelect*, DOI:10.1002/slct.202202838.

8 Y.-H. Han, M. J. Heeg and C. H. Winter, Permercuration of Ferrocenes and Ruthenocenes. New Approaches to Complexes Bearing Perhalogenated Cyclopentadienyl Ligands, *Organometallics*, 1994, **13**, 3009–3019.

9 P. Jutzi and N. Burford, Structurally Diverse π-Cyclopentadienyl Complexes of the Main Group Elements, *Chem. Rev.*, 1999, **99**, 969–990.

10 T. F. C. Cruz, K. Shimizu, J. M. S. S. Esperança, V. André, M. T. Duarte, L. P. N. Rebelo, P. T. Gomes and J. N. Canongia Lopes, Ionic Liquids in Wonderland: From Electrostatics to Coordination Chemistry, *J. Phys. Chem. C*, 2019, **123**, 5804–5811.

11 T. F. C. Cruz, K. Shimizu, J. M. S. S. Esperança, L. P. N. Rebelo, P. T. Gomes and J. N. Canongia Lopes, ILs through the looking glass: electrostatics and structure probed using charge-inverted ionic liquid pairs, *Faraday Discuss.*, 2018, **206**, 203–218.

12 P. E. Bender, D. Hill, P. H. Offen, K. Razgaitis, P. Lavanchy, O. D. Stringer, B. M. Sutton, D. E. Griswold and M. DiMartino, 5,6-Diaryl-2,3-dihydroimidazo[2,1-b]thiazoles: a new class of immunoregulatory antiinflammatory agents, *J. Med. Chem.*, 1985, **28**, 1169–1177.

13 F. Bellina and R. Rossi, Regioselective Functionalization of the Imidazole Ring via Transition Metal-Catalyzed C-N and C-C Bond Forming Reactions, *Adv. Synth. Catal.*, 2010, **352**, 1223–1276.

14 M. García-Olave, N. R. Elejalde-Cadena, J. Portilla and M. A. Macías, C–H···X (X = F, Cl) and Cl···Cl halogen-mediated interactions driving the crystal packing in N-substituted 4-arylimidazoles, *J. Mol. Struct.*, DOI:10.1016/j.molstruc.2022.134181.

15 K. J. Evans and S. M. Mansell, Functionalised N-Heterocyclic Carbene Ligands in Bimetallic Architectures, *Chem. - A Eur. J.*, 2020, **26**, 5927–5941.

16 E. Peris, Smart N-Heterocyclic Carbene Ligands in Catalysis, *Chem. Rev.*, 2018, **118**, 9988–10031.

17 I. Avinash, V. Gupta, V. Karthik and G. Anantharaman, A straightforward synthesis of 4,5-dihalofunctionalized imidazol-2-ylidene/imidazolyl-metal complexes from trihaloimidazolium salts/imidazoles: Structure and catalytic studies, *J. Organomet. Chem.*, 2017, **851**, 104–114.

18 K. Tan, C. Li, H. Meng and Z. Wang, Improvement of Hydrophobicity of Ionic Liquids by Partial Chlorination and Fluorination of the Cation, *Chinese J. Chem.*, 2009, **27**, 174–178.

19 C. Ye and J. M. Shreeve, Syntheses of Very Dense Halogenated Liquids, *J. Org. Chem.*, 2004, **69**, 6511–6513.

20 T. Mukai and K. Nishikawa, 4,5-Dihaloimidazolium-based ionic liquids: Effects of halogen-bonding on crystal structures and ionic conductivity, *RSC Adv.*, 2013, **3**, 19952–19955.

21 M. Andrzejewski, J. Marciniak, K. W. Rajewski and A. Katrusiak, Halogen and Hydrogen Bond Architectures in Switchable Chains of Di- and Trihaloimidazoles, *Cryst. Growth Des.*, 2015, **15**, 1658–1665.

22 T. Mukai and K. Nishikawa, Syntheses and crystal structures of two ionic liquids with halogen-bonding groups: 4,5-dibromo- and 4,5-diiodo-1-butyl-3-methylimidazolium trifluoromethanesulfonates, *Solid State Sci.*, 2010, **12**, 783–788.

23 T. Mukai and K. Nishikawa, Crystal Structure of 1-Methyl-2,4,5-triiodoimidazole: Formation of a Triangular Trimer through Halogen Bonding, *X-ray Struct. Anal. Online*, 2013, **29**, 13–14.
24 T. Mukai and K. Nishikawa, Halogen-bonded and Hydrogen-bonded Network Structures in Crystals of 1-Propyl- and 1-Butyl-4,5-dibromo-3-methylimidazolium Bromides, *Chem. Lett.*, 2009, **38**, 402–403.
25 T. Peppel, C. Roth, K. Fumino, D. Paschek, M. Köckerling and R. Ludwig, The Influence of Hydrogen-Bond Defects on the Properties of Ionic Liquids, *Angew. Chemie Int. Ed.*, 2011, **50**, 6661–6665.
26 K. Fumino, T. Peppel, M. Geppert-Rybczyńska, D. H. Zaitsau, J. K. Lehmann, S. P. Verevkin, M. Köckerling and R. Ludwig, The influence of hydrogen bonding on the physical properties of ionic liquids, *Phys. Chem. Chem. Phys.*, 2011, **13**, 14064.
27 C. E. S. Bernardes and J. N. Canongia Lopes, Modeling Halogen Bonds in Ionic Liquids: A Force Field for Imidazolium and Halo-Imidazolium Derivatives, *J. Chem. Theory Comput.*, 2017, **13**, 6167–6176.
28 Japan Patent Office (日本国特許庁), 4500523, 2010, 1–9.
29 A. Grineva, O. Filippov, S. Nefedov, N. Lugan, V. César, A. Grineva, O. Filippov, S. Nefedov, N. Lugan, V. César, D. Access, A. A. Grineva, O. A. Filippov, S. E. Nefedov, N. Lugan, V. César and D. A. Valyaev, Direct Access to IMes F and IMes F 2 by Electrophilic Fluorination of Abnormal N-Heterocyclic Carbenes To cite this version : HAL Id : hal-02333068 Direct Access to IMes F and IMes F 2 by Electrophilic Fluorination of Abnormal N-Heterocyclic Carbenes.
30 M. Ohashi, K. Ando, S. Murakami, K. Michigami and S. Ogoshi, N -Heterocyclic Carbenes with Polyfluorinated Groups at the 4- and 5-Positions from [3 + 2] Cycloadditions between Formamidinates and cis -1,2-Difluoroalkene Derivatives, *J. Am. Chem. Soc.*, 2023, **145**, 23098–23108.
31 A. J. Arduengo, R. Krafczyk, R. Schmutzler, H. A. Craig, J. R. Goerlich, W. J. Marshall and M. Unverzagt, Imidazolylidenes, imidazolinylidenes and imidazolidines, *Tetrahedron*, 1999, **55**, 14523–14534.
32 S. K. Furfari, M. R. Gyton, D. Twycross and M. L. Cole, Air stable NHCs: A study of stereoelectronics and metallorganic catalytic activity, *Chem. Commun.*, 2015, **51**, 74–76.
33 C. E. S. Bernardes, K. Shimizu, A. I. M. C. Lobo Ferreira, L. M. N. B. F. Santos and J. N. Canongia Lopes, Structure and Aggregation in the 1,3-Dialkyl-imidazolium Bis(trifluoromethylsulfonyl)imide Ionic Liquid Family: 2. From Single to Double Long Alkyl Side Chains, *J. Phys. Chem. B*, 2014, **118**, 6885–6895.
34 K. Shimizu, C. E. S. Bernardes and J. N. Canongia Lopes, Structure and aggregation in the 1-alkyl-3-methylimidazolium bis(trifluoromethylsulfonyl)imide Ionic Liquid homologous series, *J. Phys. Chem. B*, 2014, **118**, 567–576.
35 K. Matsumoto, R. Hagiwara, R. Yoshida, Y. Ito, Z. Mazej, P. Benkič, B. Žemva, O. Tamada, H. Yoshino and S. Matsubara, Syntheses, structures and properties of 1-ethyl-3-methylimidazolium salts of fluorocomplex anions, *Dalt. Trans.*, 2004, 144–149.
36 G. Kaminski, E. M. Duffy, T. Matsui and W. L. Jorgensen, Free Energies of Hydration and Pure Liquid Properties of Hydrocarbons from the OPLS All-Atom Model, *J. Phys. Chem.*, 1994, **98**, 13077–13082.